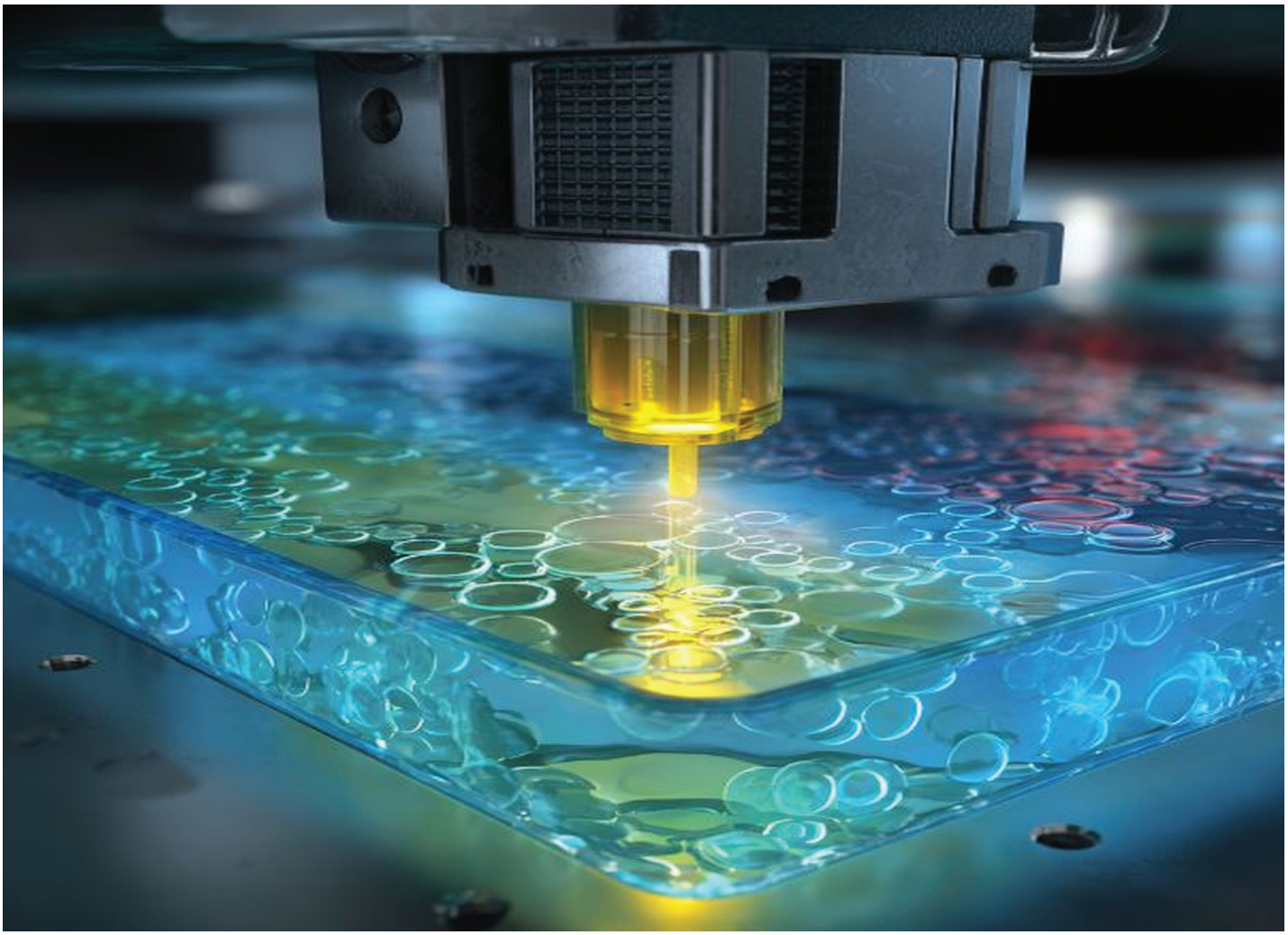

Showcasing research from Professor Jeff Bates's laboratory, Department of Materials Science & Engineering, University of Utah, Salt Lake City, Utah, USA.

Cost-effective BioInk design *via* additive tuning: a cross-platform strategy for 3D bioprinting

This research presents a cost-effective strategy for designing 3D printing BioInks by tuning additives in polyethylene glycol diacrylate-based formulations. The study demonstrates how changing molecular weights and incorporating diverse photo-initiators and rheological modifiers enables customizable mechanical and optical properties across stereolithography, DLP, and extrusion platforms. Results show significant cost reductions—up to 65%—compared to commercial controls, while maintaining biocompatibility and print fidelity for additive manufacturing.

Image reproduced by permission of Ashwin Velraj, Ethan Hathaway and Jeffrey Bates from *RSC Appl. Polym.*, 2026, **4**, 218.

Image generated using Microsoft Copilot (Enterprise version).

As featured in:

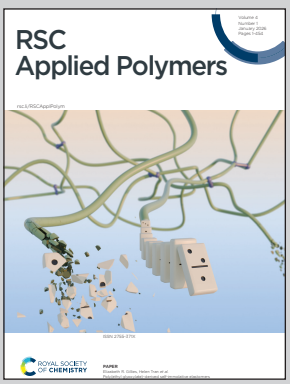

See Jeffrey Bates *et al.*, *RSC Appl. Polym.*, 2026, **4**, 218.

ROYAL SOCIETY OF CHEMISTRY

rsc.li/RSCApplPolym

Registered charity number: 207890

RSC Applied Polymers

ROYAL SOCIETY OF CHEMISTRY

PAPER

View Article Online
View Journal | View Issue

Cite this: *RSC Appl. Polym.*, 2026, **4**, 218

Cost-effective BioInk design *via* additive tuning: a cross-platform strategy for 3D bioprinting

Ashwin Velraj, Ethan Hathaway and Jeffrey Bates *

Received 24th June 2025,
Accepted 19th September 2025

DOI: 10.1039/d5lp00190k

rsc.li/rscapplpolym

Custom biomaterials as inks for 3D printing (BioInks) are recently being explored to curate features to eliminate device failures caused by structural delamination. This study investigated BioInks composed of polyethylene glycol diacrylates of varying molecular weights for their inherent swelling, soft mechanical strength, non-reactivity, and biocompatibility. These BioInks have been tuned to be photo-sensitive to a range of wavelengths using a panel of photo-initiator and photo-absorber additives. Modifying visco-elastic and UV-sensitive properties yields cross-platform BioInk compositions that can be printed across stereolithography (SLA), digital light processing (DLP), and direct ink extrusion technologies. We also explore the cost efficiencies of using alternative photo additives to improve accessibility and affordability. 3D-printed techniques employing multilayered constructs are great candidates for fabricating biomedical devices that exhibit controlled reactions triggered by analyte molecules and shear or compressive pressure changes in their microenvironment as experienced within target organs in the body.

Introduction

Hydrogels are flexible biomaterials that can be customized for various uses in tissue engineering and drug delivery due to their adjustable characteristics and ability to interact with biological systems.[1–3] The emergence of additive manufacturing methods, such as 3D printing, has transformed manufacturing abilities, allowing for the creation of complex designs and structures in different sectors like automotive, aerospace, and biomedical engineering.[4–6] Significant progress in materials science, printing methods, and biofabrication techniques has greatly improved the application of 3D printing for hydrogels, enabling the creation of intricate designs with accurate management of both structure and function.

A key obstacle in 3D printing is choosing appropriate materials with the right printing capabilities, mechanical properties, and functionality for particular uses.[6–9] The importance of 3D printing using polymers in the medical field is substantial for creating customized implants, drug delivery methods, and tissue-engineered frameworks.[10–12] Novel hydrogel formulations have been created with unique mechanical properties, compatibility with living organisms, and the ability to adapt to environmental changes.[13–16] This includes combining hybrid hydrogel composites with bioactive molecules, nanoparticles, or reinforcement materials to improve mechanical strength, conductivity, and bioactivity.[17–20] Progress in material design allows the creation of hydrogel-based structures with tailored characteristics for particular biomedical uses.

Innovations in printing techniques like stereolithography (SLA) and digital light processing (DLP) have made it possible to print precise hydrogel structures with complex shapes and minuscule details.[21–24] Printing systems that use controlled light exposure or direct precision injection enable accurate control over deposition variables, which enables the creation of intricate 3D structures with unique mechanical characteristics.[25,26] These methods present fresh possibilities for crafting custom implants and tissue scaffolds tailored to each patient with enhanced accuracy and genuineness. Various 3D printing methods, such as inkjet printing and extrusion, allow the integration of multiple hydrogel formulas or materials in one printed object.[25,26] Multi-material printing allows for the creation of intricate biomimetic structures with various functions.[27–29]

3D printing of hydrogels has progressed to create intricate tissues and organs with anatomically accurate structures and physiological functions. Combining cells, growth factors, and biomimetic scaffolds in printed structures allows for replicating tissue environments and supporting tissue regeneration and formation of organoids.[30] Bioprinting shows potential for use in regenerative medicine, modeling diseases, and screening personalized drugs.[7,31,32] The ability of a polymer to be processed into specific shapes with high accuracy and faithfulness is essential for successful 3D printing.[33,34]

Evaluation of printability includes a set of tests to analyze the polymer's flow characteristics, ability to be extruded, and overall printing performance in comparison to other polymers

Department of Materials Science & Engineering, University of Utah, Salt Lake City, Utah, USA. E-mail: jeff.bates@utah.edu

used in 3D printing. Rheology provides insight into the flow properties of the polymeric formulations, which is essential for techniques involving extrusion-based 3D printing.[33,35,36] Measurements of viscosity at various shear rates and viscoelastic properties through oscillatory rheometry can help understand how the material will behave during printing. Extrusion printing techniques require the testing of factors that affect print quality, such as extrusion force, nozzle diameter, and relaxation after shear, through a combination of rheology and visual evaluation of successful prints.[33,34,36–38] These determine the material's suitability for printing. Mechanical testing assesses the performance, stability, time to failure, and structural integrity of printed constructs.

All 3D printing techniques build a construct from the ground up in a layer-by-layer method, building along the *x*-*y* plane, one layer at a time. Interlayer adhesion is crucial between printed layers, which is crucial for structural integrity and avoiding delamination.[34] Lap tests, peel shear tests, or tack tests provide the necessary insight into the adhesive and cohesive properties of printing formulations. Cross-platform printability assessments involve printing similar structures using various 3D printing techniques such as photocuring-based printing and extrusion printing and comparing the quality of the prints in terms of layer adhesion, surface finish, precision across repeated prints, and dimensional accuracy. Maintaining cell viability, functionality, and spatial arrangement in printed tissues is a crucial challenge for the success of tissue engineering applications.[39,40] Biocompatibility, ensuring long-term stability, and addressing regulatory concerns are crucial aspects to consider when translating 3D-printed hydrogel-based implants and medical devices into clinical settings.[24,41]

In this study, polymeric formulations using known biocompatible compounds are modified to achieve printability across different types of 3D printers incorporating light and extrusion-based 3D printers. Each printer presents a different loading volume requirement, flow rate, viscosity requirement and curing parameter, to which proprietary resin properties are tuned. The goal is to optimize printability of in-house polymeric BioInk formulations across different 3D printing techniques commonly used in medical settings to achieve broad compatibility.

In conclusion, the latest advancements in 3D printing of hydrogels show significant potential for progressing tissue engineering, drug delivery, and personalized medicine. Continuous research is essential to address existing obstacles and fully unlock the capabilities of this technology for medical purposes. Progressing improvements in material design, printing methods, and biofabrication strategies will propel innovation and support the creation of next-generation hydrogel-based treatments and devices.

Materials and methods

The BioInks were prepared using combinations of polyethylene glycols, acrylates, acrylamides, and sodium alginate to tune sensitivities to desired analyte molecules. When printing with light-based printers, 40% w/v acrylate-based backbones in deionized water are chosen with up to 3% w/v photo-additives (at 10 : 1 ratio of photo-initiator to photo-absorber specifically) sensitive to the 390 nm–410 nm range. Photo-initiator concentrations were reverse calculated against standard curves established using serial dilutions of commercial resins on a Scilogex SCI-V1100 Spectrophotometer.

The total volume of the batch made for final printing depends on the printer used, ranging from 1 mL to 500 mL. A combination of Pneumatic Air Extrusion-based CellInk BioX, DLP-based CellInk LumenX, and SLA-based Formlabs Inc Form 3 printers were used to print these constructs. The LumenX was the primary printer of choice for obtaining hydrogel-based trays and seamless hydrogel tubes, which were both the sensing and reservoir elements of the constructs. The BioX printer was used in two ways: (1) to fill a secondary hydrogel element into the constructs printed and (2) to print a 2-part hydrogel construct consisting of monomer-crosslinker complexes and accelerators. The Form 3 printer demonstrated the cross-platform functionality of the modified BioInks created in-house for CellInk printer projects.

Commercial resin compositions printed using the three 3D printers, were used as controls for this research. Both these resins are proprietary variations containing unknown concentrations of polymeric backbones, photo-initiators and photo-absorbers. These represent the current industry standards and our in-house BioInk samples were compared to properties exhibited by these controls. Sample compositions were made using PEGDA (polyethylene glycol diacrylates; molecular weight of 700 Daltons) as the primary backbone and additives such as PEG 400 (polyethylene glycol; molecular weight 400 Daltons), AAM (acrylamide), FS (fumed Silica) or HEMA (hydroxyethyl methacrylate) with photo additives (photo-initiator-photo-absorber at a ratio of 10 : 1). A range of custom photo-initiators such as I2959(2-hydroxy-4′-(2-hydroxyethoxy)-2-methylpropiophenone), DMPAP (2,2-dimethoxy-2-phenylacetophenone), VA-086 (2,2′-azobis[2-methyl-*N*-(2-hydroxyethyl) propionamide]), CQ (camphorquinone), CTX (2-chlorothioxanthen-9-one), MK (4,4′-bis(dimethylamino) benzophenone) were compared against commercially used LAP (lithium phenyl-2,4,6-trimethylbenzoylphosphinate). Tartrazine, a biocompatible yellow azo dye, was chosen as the photo-absorber to minimize light scattering and prevent the curing of non-printed areas.

Compositions were all made to a set 4 mL total volume to control for synthesis variables and negate discrepancies such as stirring, vortexing, mechanical agitation, diffusion or precipitation. Photo-initiator stocks were premade at a concentration of 10% w/v dissolved in appropriate solvents due to their sensitivities once added to light-cured polymeric backbones. Solutes with a lower dissolution rate were ultrasonicated in a water bath-sonicator for 60 seconds to ensure dissolution into the solvent. Photo-initiators and photo-absorbers were added to the formulation at volumetric concentrations varying from 1% to 3% w/v before loading into the 3D printer.

0.5 mL of the formulated resins are spot-tested for cross-linking under handheld irradiation of different UV wavelengths and curing time. A post-print conditioning was done where the constructs were cyclically washed for 1 hour in deionized water and 10% v/v ethanol in deionized water solution to elute any unreacted monomers or additives. Photo-curability of initial formulations were tested to verify that the photo-additives enabled curing at the parameters available on the printers. Further optimizations were stepwise adjustments to ensure resin filling into the printer's load tanks through flow valves, adherence to print-bed surfaces, and successful extrusion through nozzles under shear force. Successful polymerizations indicated the ability to use the tested formulation in UV light-based 3D printing platforms such as SLA & DLP. Following this, flow and deformation tests are characterized on an Anton Paar MCR 302 Modular Compact Rheometer to ascertain their ability to be extruded through 3D printing platforms such as material jetting and pneumatic air extrusion (Table 1).

All chemicals used in this study were purchased from Sigma Aldrich and Fisher Scientific. Resins used as controls were purchased directly from 3D printer manufacturers. Costs for analysis and comparisons were calculated based on market costs of chemicals and control resins between fiscal years 2022–2024. All tests were run on triplicates, and error bars represent the standard error of the mean. All data were graphed and statistically analyzed using GraphPad Prism version 10.2.3 for Windows, GraphPad Software.

Results and discussion

Light and extrusion-based 3D printers were assessed for their printing parameters such as UV wavelengths, light intensities, print speeds, shear rates and layer thicknesses. Formulations fabricated in this study were assessed for their properties and compared to commercial resin, referred to as 'controls'. For light-based printing inks, the samples were spot-tested for their sensitivity to UV wavelengths of 365 nm and 405 nm irradiated between 20–30 mW cm^{-2} up to a working distance of up to 2 inches from the irradiation source, which is typical of SLA and DLP printers. Success was based on observation of complete transition of polymer solution to sol–gel constructs without defects or inconsistencies. As seen in Fig. 1 (left) the samples successfully cured under 15 s, showing sensitivity to these parameters with most formulations curing well within 10 seconds and showing no significant difference compared to controls in their curing time, as seen in Fig. 1 (right).

For extrusion-based printing inks, the samples were tested for their viscosity, extrudability, and tack. Samples were tested before and after the addition of rheological modifiers, as initial unmodified formulations showed that the tack showed significant differences to controls, as seen in Fig. 2 (left). Tack determines the adhesion of the first printed later to the build platform and the cohesion of subsequent print layers to the previous layers. Fig. 2 (right) shows that the modified resins have comparable values of tack showed by the normal force required to detach the measuring tool from the material, verified by the lack significant differences comparing all controls to modified samples seen in Fig. 2 (left).

Additionally, Fig. 2 (right) also shows that both control and sample resins exhibit varying levels of elasticity seen by the higher gap values before detachment attributing to higher viscosities. For both light-based and extrusion-based printing techniques, viscosity acts as a key parameter to ensure print success. Controls were found to have varying flow profiles depending on the 3D printer of interest. Controls from SLA printers have a higher viscosity while DLP resins tend to have a lower viscosity, based on the applications that these printers are intended for. Extrusion printing resins tend to focus on the shear-thinning behavior to allow for a stable loading into syringes and uninterrupted flow upon application of up to 30 kPa of normal shear force during printing. Fig. 3 shows that the viscosities of printing resins decreased upon increasing shear rates, confirming shear thinning behavior. Commercial additive manufacturing techniques, including 3D printing, use extrusion syringes or vat filling systems where formulations experience a shear rate of up to 60/s^{-1}. All tested resins show a sufficient reduction in viscosity to enable filling and shear flow.

With the selective addition of rheological modifiers based on high molecular weight PEG chains and silicates, the shear thinning profiles of the samples either matched or were

Table 1 Summary table listing all control and sample composition, sources and modifications

	Label	Source	Composition	Modifiers	Photo-additives
Controls	C1	Commercial SLA resin	Flexible (as-procured)	—	—
	C2	Commercial DLP resin	Start gel (as-procured)	—	—
	C3	Commercial DLP resin	High stiffness (as-procured)	—	—
	C4	Commercial DLP resin	Low stiffness (as-procured)	—	—
	C5	Commercial Extrusion resin	High viscosity (as-procured)	—	—
	C6	Commercial Extrusion resin	Low viscosity (as-procured)	—	—
Samples	S1	Made in-house	40% PEG-DA backbones	—	1.5%
	S2	Made in-house	20% PEG-DA backbones	5% HEMA	3%
	S3	Made in-house	40% PEG-DA backbones	2.5% HEMA	3%
	S4	Made in-house	20% PEG-DA backbones	5% silicates	1.5%
	S5	Made in-house	20% PEG-DA backbones	5% silicates	3.0%
	S6	Made in-house	20% PEG-DA backbones	8% silicates	1.5%

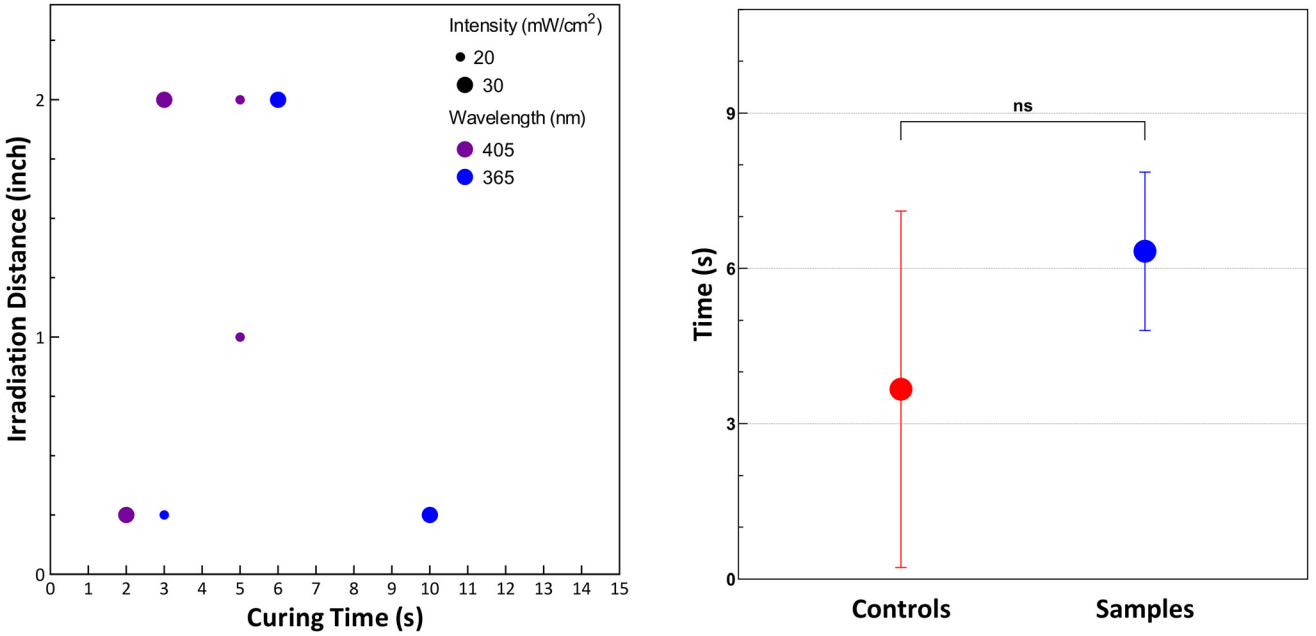

Fig. 1 Tests for the photocurable property of the light-sensitive formulations (left) samples were exposed to UV wavelengths at varying intensities for up to 30 seconds, and (right) time to complete curing in seconds compared to commercial compositions using Student's *t*-tests showed no significant difference (marked as 'ns' for a *p*-value > 0.05), showing that all compositions cured within similar exposure times.

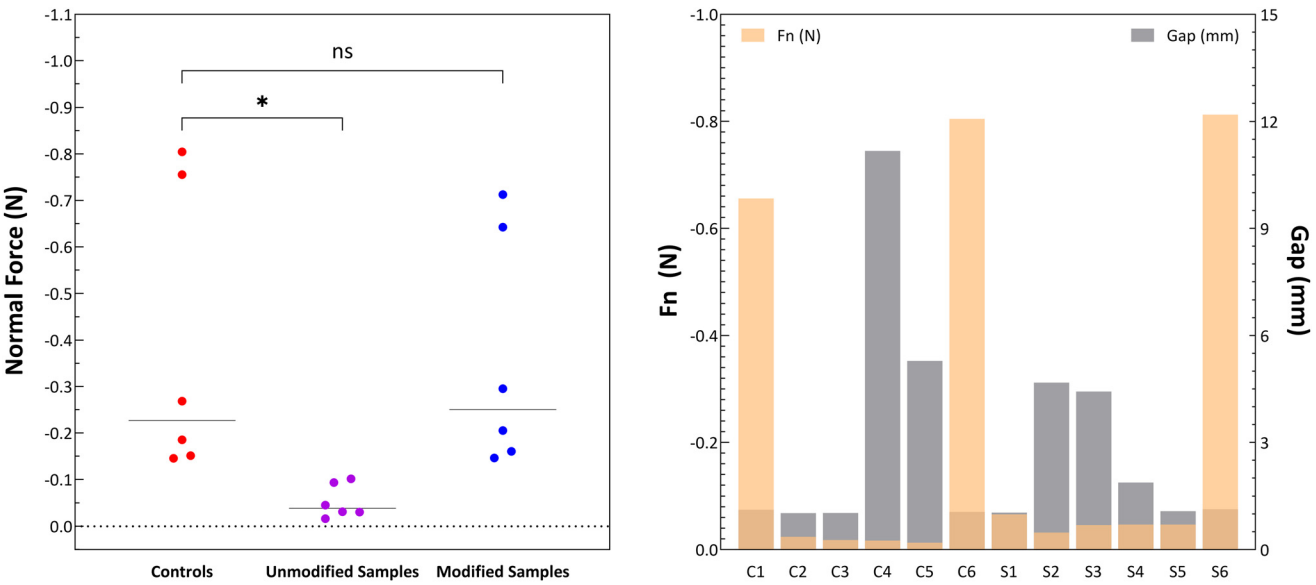

Fig. 2 Tack tests (left) before any viscosity modification shows significant differences upon the comparison of means using One-way ANOVA test groups, where significance was established at *p*-value < 0.05. After addition of rheological modifiers, a comparison of means showed no significant difference (marked as 'ns' for a *p*-value > 0.05), showing that there was no significant difference in tack between the controls and samples (right) Control resins from were tested along with formulated samples with the normal force of adhesion represented on the left *y*-axis and the distance of separation before release on the right *y*-axis.

lowered than the controls, as desired. Fig. 3 (left) shows that the low-viscosity profiles of samples used in DLP printing are highly similar to the controls, establishing the higher concentrations of PEGDA found in the control resins. Fig. 3 (right) shows that high-viscosity profiles of samples used in SLA printing showed an initial high value of viscosity followed by sharp viscosity upon application of shear force, making them ideal for extrusion-based printing as well. The versatility of extrusion printers allows setting higher pressure parameters on the interface to print formulations with varying viscosities.

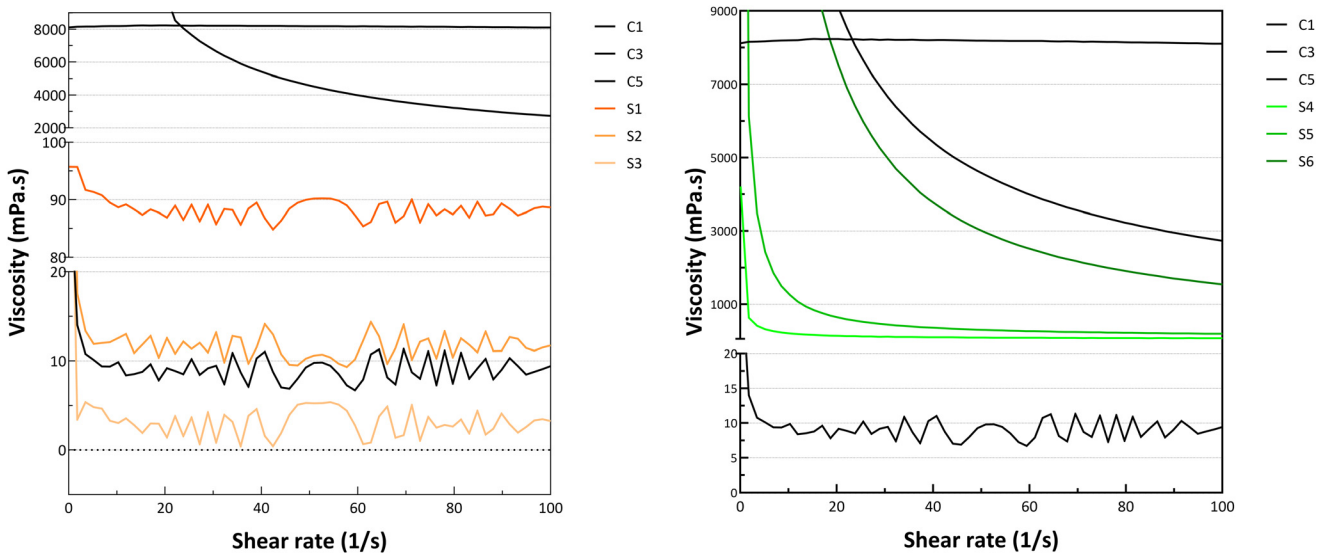

Fig. 3 Rheological viscosity under increasing shear rate profiles of (left) sample resins with lower viscosity and (right) resins with higher viscosities were compared to respective control resins to establish shear-thinning nature and sufficient reduction of viscosity upon application of shear forces by the printers.

A cost analysis of the compositions showed that the photo-initiators contribute to most of the cost incurred of the total print. Table 2 lists the retail cost per gram of resin in combination with LAP as a photo-initiator used in controls, which is the commercial photo-initiator of choice due to its ease of solubility in deionized water and quick response to 405 nm UV radiation. In comparison to commercial controls, cost of printing the custom in-house samples reduced by approximately 60%, 40% and 65% per print for DLP, extrusion and SLA printing, respectively.

The sample formulations were then printed across different 3D printing technologies, specifically the extrusion-based CellInk BioX extrusion printer and light-based Volumetric LumenX and Formlabs Form 3 printers. Fig. 4 shows multi-layered hydrogel constructs, channel layers, hollow tubes, and flexible gels across 3D printers.

The toxicity values of certain photo-initiators were obtained from published materials safety data sheets, and LD_{50} values were calculated out to 150 g of photo-initiator for an average person weighing 75 kg to assess w/w concentration comparisons.[42,43] The loading concentrations at 1%–5% w/v in these printing inks were between 0.01 g–0.05 g of photo-initiator for every mL of formulated resin, which is less than 0.04% of the toxicity value. MK, as a photo-initiator, was avoided due to its published potential carcinogenicity.[44]

Certain knowledge gaps were identified, such as the inability to simultaneously establish the irradiation distance and intensity of the embedded light processing units within the printers. Declared values obtained from technical specification sheets were used to establish the testing range for all modified formulations. Tunable printing parameters were obtained from the 3D printers available, and testing parameter ranges were chosen to match the setting required for commercial prints. 3D printed samples were additionally subjected to post-cure conditioning in deionized water to elute unreacted polymeric monomers. The lack of complete knowledge of the components of control resins due to proprietary regulations restricts the ability to account for all costs involved in fabricat-

Table 2 A cost analysis of the amount of photo-initiator added to resins for printing and the comparative costs incurred in the commercial controls against samples formulated in-house

	Printer	Technique	Composition	Loading volume per print (mL)	Cost (per mL in USD)	Cost per print (USD)
Controls	LumenX	DLP	As-procured	1	$10	$10
	BioX	Extrusion	As-procured	3	$10	$30
	Form 3	SLA	As-procured	300	$0.2	$60
Samples	LumenX	DLP	20% backbone + 1.5% photo-additives	1	$4	$4
	BioX	Extrusion	40% backbone + 3% photo-additives	3	$6	$18
	Form 3	SLA	40% backbone + 1% photo-additives	300	$0.07	$21

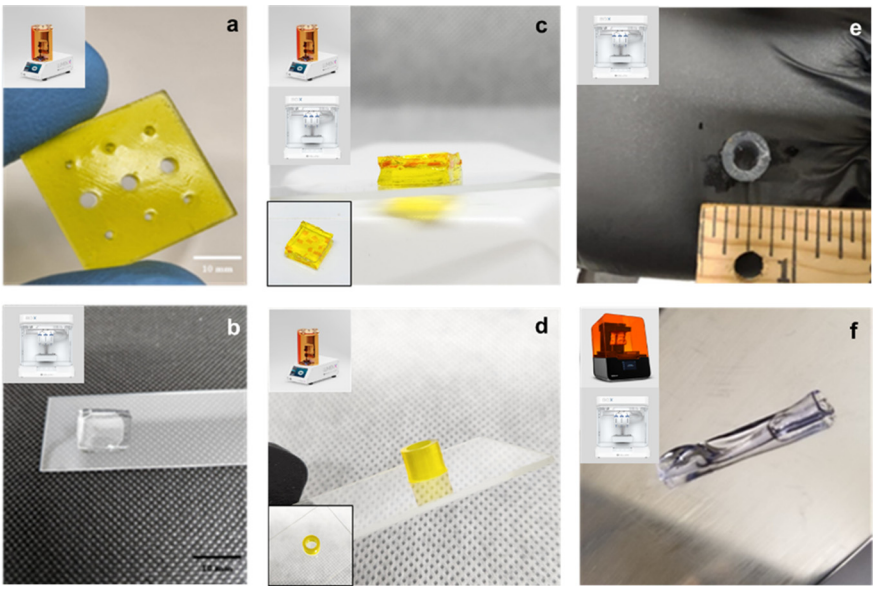

Fig. 4 The inset picture on the top left of each image shows the printer used in printing the construct shown in the respective image. (a) Channel layers showing aperture variations due to swelling in the analytic environments. (b) A capping layer can be printed as an enclosure over the multi-layered gel with extrudable polymer compositions. (c) Multilayered gel showing sandwiched loading of release moiety. (d) Printed seamless tubes allow for dynamic swelling across the inner–outer lumen in fluidic environments and loaded-dye release over time through elution. (e) & (f) Tubes of varying mechanical stiffnesses and pressure sensitivities can be printed using combinatory techniques.

ing the resin. Additionally, all cost calculations were performed based on retail costs of equivalent components or partially known components from printer manufacturers and chemical suppliers.

Conclusions

Customized formulations were successfully printed across the extrusion, SLA, and DLP platforms. Formulations used to obtain these prints were tested before and after printing. Prepolymer solutions were characterized for the viscosity and gelling times close to 1000 cP and 5 s, respectively, to match those of the commercial BioInks. The adhesion and cohesion through tack testing were released to be comparable to commercially successful resins. The gels were successfully printed across the mentioned 3D printing platforms after confirming shear-thinning and self-adhesion properties *via* rheological profiles. Scalability and reproducibility were inherently confirmed upon scaling up modified BioInks from 3 mL to 300 mL batches based on individual printer's loading volume requirements. The structure–property relationship-based response of these gels will be captured using thin-film piezo-resistive pressure-sensing circuitry displayed on a digital monitor and recorded for future work. Toxicity values from materials data safety sheets showed that the photo-additives do not pose a hazard to the overall formulation, even in the event of complete elution at the target site. Cost analyses of the printing inks revealed that the photo-additives are the most expensive constituents out of all the components. The v/v comparison between current commercial printing resins and our resins showed a reduction between 45% and 65% of the cost for every successful print depending on the printing technique, greatly improving accessibility to healthcare and clinical care facilities. Future work will focus on evaluating post-cure oscillatory rheology, swelling ratios, layer adhesion, and mechanical stiffness on a case-by-case basis, tailored to the intended biomedical device, target site, therapeutic application, and specific performance requirements.

In summary, conventional methods of BioInk preparation involve the chemical modification of materials, especially polymers, to introduce a controllable sensitivity of UV wavelengths. Our approach omits the need for modification, followed by characterization and regulatory assessments, instead using pre-approved additives to enable easy adaptions of various polymeric formations as BioInks for printing complex structures across 3D printing platforms.

Author contributions

Prof. Jeffrey Bates: conceptualization (equal); supervision; funding acquisition; validation; writing – review and editing (equal). Dr Ashwin Velraj: conceptualization (equal); investigation (lead); formal analysis; visualization; writing – original draft (lead) & review and editing (equal). Ethan Hathaway: investigation (supporting); writing – original draft (supporting).

Conflicts of interest

The authors declare they have no conflict of interest.

Data availability

Datasets for this article are available at "BioInks Characterization DataSet", Velraj, Ashwin (2025), Mendeley Data, V1, at https://doi.org/10.17632/z38f3jzhbg.1.

Acknowledgements

The authors acknowledge the Office of the Vice President for Research, Department of Materials Science & Engineering, and Price College of Engineering FY23 SEED Award at the University of Utah, Salt Lake City, Utah, USA, for funding this work. The authors acknowledge CellInk for providing the BioX bioprinter for extrusion printing techniques explored in this study.

During the preparation of this work, the lead author used the ChatGPT (GPT-3.5) model, OpenAI (2023), in order to obtain and arrange points of discussion for parts of the introduction section only. After using this tool/service, the lead author reviewed and edited the content as needed and takes full responsibility for the content of the publication.

References

1 N. B. Day, R. Dalhuisen, N. E. Loomis, S. G. Adzema, J. Prakash and C. W. Shields IV, *Acta Biomater.*, 2022, **150**, 211–220.
2 J. Chen, J. Yang, L. Wang, X. Zhang, B. C. Heng, D. A. Wang and Z. Ge, *Bioact. Mater.*, 2021, **6**, 1689–1698.
3 M. M. Rana and H. D. la H. Siegler, *Gels*, 2024, **10**, 216.
4 L. Y. Zhou, J. Fu and Y. He, *Adv. Funct. Mater.*, 2020, **30**, 2000187.
5 K. Deshmukh, M. T. Houkan, M. A. A. AlMaadeed and K. K. Sadasivunid, *3D and 4D Printing of Polymer Nanocomposite Materials: Processes, Applications, and Challenges*, 2019, pp. 1–24.
6 N. Shahrubudin, T. C. Lee and R. Ramlan, *Procedia Manuf.*, 2019, **35**, 1286–1296.
7 Z. Liu, Y. Wang, B. Wu, C. Cui, Y. Guo and C. Yan, *Int. J. Adv. Des. Manuf. Technol.*, 2019, **102**, 2877–2889.
8 V. Tsioukas, C. Pikridas and I. A. Karolos, *3D Printing: Applications in Medicine and Surgery*, 2020, pp. 151–155.
9 S. F. Iftekar, A. Aabid, A. Amir and M. Baig, *Polymers*, 2023, **15**, 2519.
10 M. Guvendiren, J. Molde, R. M. D. Soares and J. Kohn, *ACS Biomater. Sci. Eng.*, 2016, **2**, 1679–1693.
11 A. E. Jakus, A. L. Rutz and R. N. Shah, *Biomed. Mater.*, 2016, **11**, 014102.
12 J. Gopinathan and I. Noh, *Biomater. Res.*, 2018, **22**(1), 1–15.
13 V. P. Torchilin, *Nat. Rev. Drug Discovery*, 2014, **13**, 813–827.
14 C. Luo, M. Huang and H. Liu, *J. Appl. Polym. Sci.*, 2022, **139**, 51925.
15 R. Tan, Z. She, M. Wang, Z. Fang, Y. Liu and Q. Feng, *Carbohydr. Polym.*, 2012, **87**, 1515–1521.
16 M. Abbasi, M. Sohail, M. U. Minhas, S. Khan, Z. Hussain, A. Mahmood, S. A. Shah and M. Kousar, *Int. J. Biol. Macromol.*, 2019, **136**, 83–96.
17 V. B. Morris, S. Nimbalkar, M. Younesi, P. McClellan and O. Akkus, *Ann. Biomed. Eng.*, 2017, **45**, 286–296.
18 H. Chen, F. Yang, R. Hu, M. Zhang, B. Ren, X. Gong, J. Ma, B. Jiang, Q. Chen and J. Zheng, *J. Mater. Chem. B*, 2016, **4**, 5814–5824.
19 R. Zhu, D. Zhu, Z. Zheng and X. Wang, *Nat. Commun.*, 2024, **15**(1), 1–11.
20 A. M. Mathur, S. K. Moorjani, and A. B. Scranton, *J. Macromol. Sci., Part C: Polym. Rev.*, 1996, 405–430.
21 J. Huang, Q. Qin and J. Wang, *Processes*, 2020, **8**, 1138.
22 Z. Wang, R. Abdulla, B. Parker, R. Samanipour, S. Ghosh and K. Kim, *Biofabrication*, 2015, **7**, 045009.
23 I. Karakurt, A. Aydoğdu, S. Çıkrıkcı, J. Orozco and L. Lin, *Int. J. Pharm.*, 2020, **584**, 119428.
24 S. H. Kim, Y. K. Yeon, J. M. Lee, J. R. Chao, Y. J. Lee, Y. B. Seo, M. T. Sultan, O. J. Lee, J. S. Lee, S.-I. Yoon, I. S. Hong, G. Khang, S. J. Lee, J. J. Yoo and C. H. Park, *Nat. Commun.*, 2018, **9**(1), 1620.
25 N. Kumar, B. Ghosh, A. Kumar, R. Koley, S. Dhara and S. Chattopadhyay, *J. Drug Delivery Sci. Technol.*, 2023, **80**, 104111.
26 L. Jin, J. Xu, Y. Xue, X. Zhang, M. Feng, C. Wang, W. Yao, J. Wang and M. He, *Gels*, 2021, **7**, 172.
27 E. Tamahkar, B. Özkahraman, A. K. Süloğlu, N. İdil and I. Perçin, *J. Drug Delivery Sci. Technol.*, 2020, **58**, 101536.
28 Z. Ma, W. Song, Y. He and H. Li, *ACS Appl. Mater. Interfaces*, 2020, **12**, 29787–29806.
29 V. Kozlovskaya, M. Dolmat and E. Kharlampieva, *Langmuir*, 2022, **38**, 7867–7888.
30 S. N. Patel, M. Ishahak, D. Chaimov, A. Velraj, D. LaShoto, D. W. Hagan, P. Buchwald, E. A. Phelps, A. Agarwal and C. L. Stabler, *Sci. Adv.*, 2021, **7**, eaba5515.
31 D. Vera, M. García-Díaz, N. Torras, M. Álvarez, R. Villa and E. Martinez, *ACS Appl. Mater. Interfaces*, 2021, **13**, 13920–13933.
32 World-first 3D bioprinted bioimpedance chips unlock *in vivo* skin disease modeling – 3D Printing Industry, https://3dprintingindustry.com/news/world-first-3d-bioprinted-bioimpedance-chips-unlock-in-vivo-skin-disease-modeling-215269/, (accessed 29 August 2023).
33 H. Herrada-Manchón, M. A. Fernández and E. Aguilar, *Gels*, 2023, **9**, 517.
34 G. Stojkov, Z. Niyazov, F. Picchioni and R. K. Bose, *Gels*, 2021, **7**, 255.
35 R. G. Ricarte and S. Shanbhag, *Polym. Chem.*, 2024, **15**, 815–846.
36 J. P. Greene, *Automotive Plastics and Composites*, 2021, pp. 57–69.
37 L. Sangroniz, M. Fernández and A. Santamaria, *Polymer*, 2023, **271**, 125811.

38 D. K. Baby, *Rheology of Polymer Blends and Nanocomposites: Theory, Modelling and Applications*, 2020, pp. 193–204.
39 W. Zhu, X. Ma, M. Gou, D. Mei, K. Zhang and S. Chen, *Curr. Opin. Biotechnol.*, 2016, **40**, 103–112.
40 F. Yang, J. Zhao, W. J. Koshut, J. Watt, J. C. Riboh, K. Gall, B. J. Wiley, F. Yang, J. Zhao, B. J. Wiley, W. J. Koshut, K. Gall, J. Watt and J. C. Riboh, *Adv. Funct. Mater.*, 2020, **30**, 2003451.
41 M. Nakamura, A. Kobayashi, F. Takagi, A. Watanabe, Y. Hiruma, K. Ohuchi, Y. Iwasaki, M. Horie, I. Morita and S. Takatani, *Tissue Eng.*, 2005, **11**, 1658–1666.
42 2-Hydroxy-1-(4-(2-hydroxyethoxy)phenyl)-2-methylpropan-1-one | $C_{12}H_{16}O_4$ | CID 86266 – PubChem, https://pubchem.ncbi.nlm.nih.gov/compound/86266, (accessed 6 January 2024).
43 2,2′-Azobis(*N*-(2-hydroxyethyl)-2-methylpropionamide) | $C_{12}H_{24}N_4O_4$ | CID 381605 – PubChem, https://pubchem.ncbi.nlm.nih.gov/compound/61551-69-7, (accessed 6 January 2024).
44 Michler's ketone | $C_{17}H_{20}N_2O$ | CID 7031 – PubChem, https://pubchem.ncbi.nlm.nih.gov/compound/Michler_s-ketone, (accessed 23 June 2024).